A LIDAR SYSTEM FOR REMOTE PROBING OF THE LOWER ATMOSPHERE

Prepared by

Charles D. Craig and Robert Bartz*

Lars E. Olsson**
Principal Investigator

E. Wendell Hewson
Chairman, Dept. of Atmospheric Sciences

Department of Atmospheric Sciences
Oregon State University
Corvallis, Oregon 97331

(NASA-CR-141013) A LIDAR SYSTEM FOR REMOTE PROBING OF THE LOWER ATMOSPHERE (Oregon State Univ.) 53 p HC $4.25 CSCL 17I

N75-13241

Unclas
G3/36 03653

November 1974

* Present Affilliation, School of Oceanography, Oregon State University.

** Present Affilliation, Swedish Meteorological and Hydrological Institute, Stockholm.

NOTE: The original version of this report was prepared in December, 1972.

TABLE OF CONTENTS

Page

LIST OF TABLES

LIST OF FIGURES

A Lidar System for the Remote Probing of the Lower Atmosphere

1. Summary

The Department of Atmospheric Sciences at Oregon State University has developed and tested a lidar* system under NASA Grant No. NGR 30-002-048.

The lidar system employs a Q-switched ruby laser that radiates an intense pulse of light into the atmosphere, thereby illuminating aerosol particles in the laser beam. Light backscattered from these particles is received by a cassegrain telescope that is equipped with a sensitive photomultiplier tube. The output signal of the photomultiplier tube is displayed with respect to elapsed time (A-scope display) on an oscilloscope and photographed on polaroid film. The film is manually digitized and subsequently processed by computer to obtain normalized apparent backscatter coefficient profiles which can be interpreted (with some assumptions) as approximate profiles of relative aerosol concentration.

The system is capable of measuring aerosol profiles to ranges greater than three kilometers.

2. System Technical Description

The lidar system is illustrated schematically in Figure 1 and pictorially in Figure 2. The lidar system characteristics are summarized in Table 1. The system consists of an azimuth and elevation positioner, optical mount, a ruby laser transmitter, an optical receiver, electronics consoles, and a data display and recording system.

---

* light detection and ranging

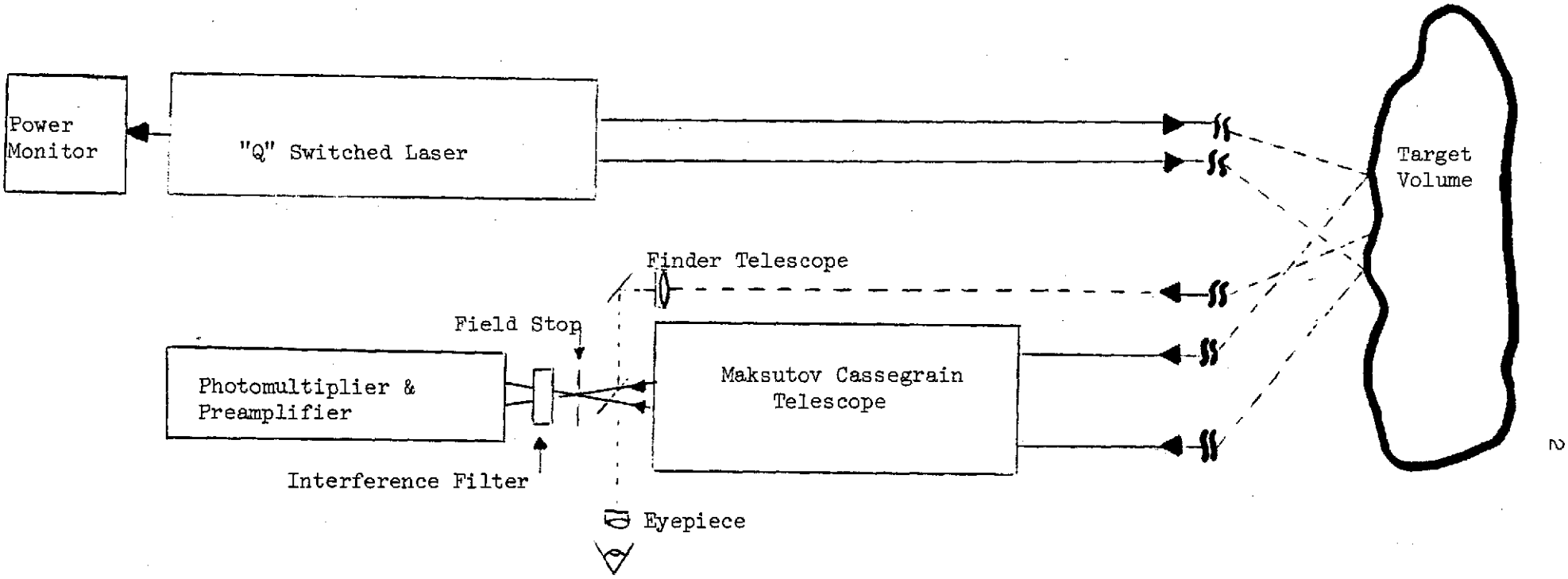

FIGURE 1. LIDAR SYSTEM SCHEMATIC

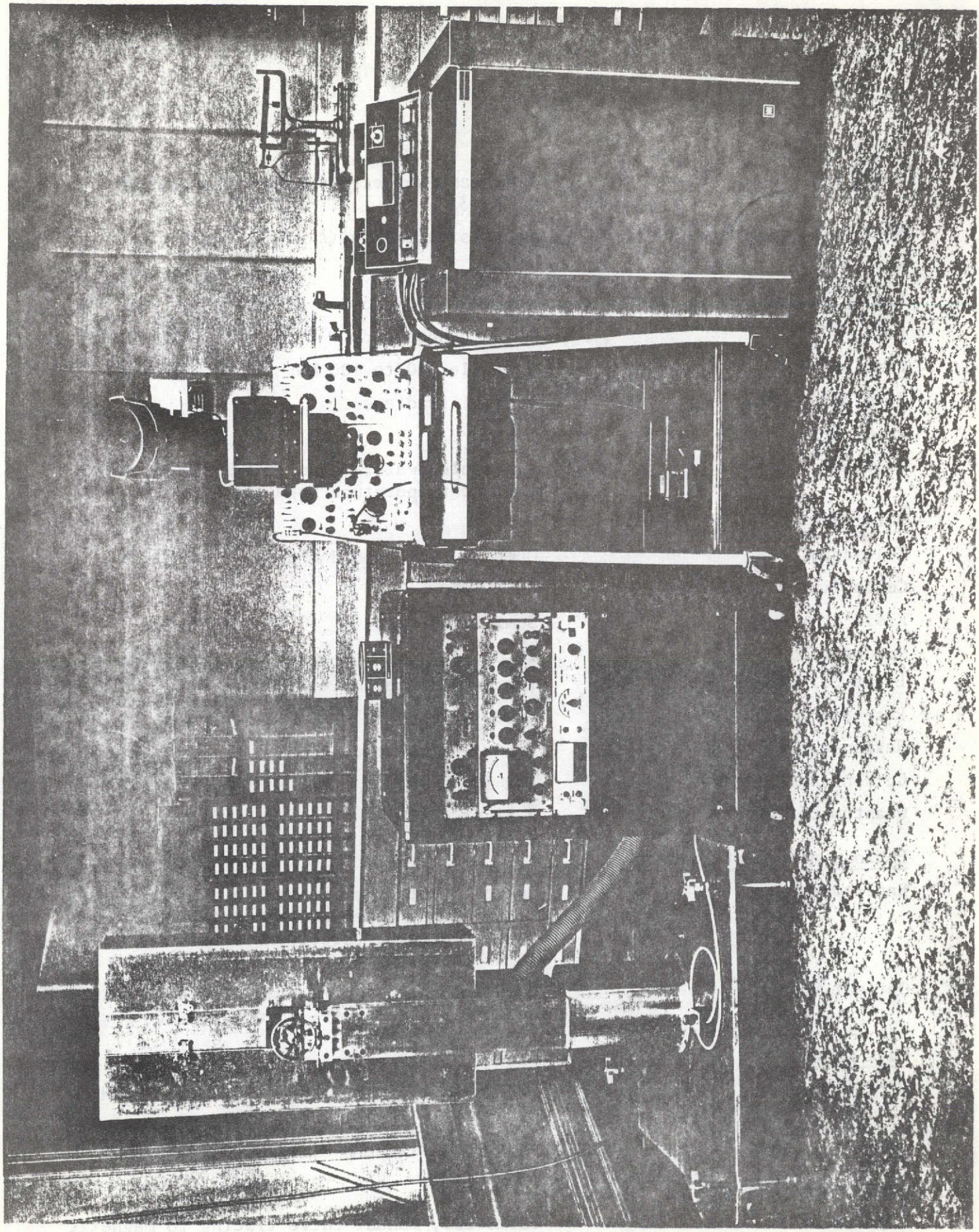

FIGURE 2. LIDAR SYSTEM

TABLE 1: LIDAR SYSTEM CHARACTERISTICS

Transmitter	
Laser type:	Holobeam, series 300, Ruby, Q-switched, model 330
Mode of Operation:	Pockels cell Q-switched
Wave Length:	6943$\mathring{A}$
Energy/Pulse:	Variable 0.2 to 2.0 joules
Pulse Width:	10-30 nanoseconds
Peak Power:	Variable 10 to 100 MW
Beam Divergence:	3.8 milliradians
Pulse Repetition Rate:	6 PPM
Cooling:	air cooled water-circulating system, above ambient temperature regulator
Receiver	
Telescope:	Questar 89 MM field model
Collecting Area:	62.2 CM^2
Field of View:	5 milliradians
Spectral Band Width:	10 nm, optics tech interference filter
Light Detector:	Photomultiplier, R.C.A., 7326
Response:	S-20
Response Time:	2.5×10^{-9} seconds
Current Amplification:	1×10^6
Quantum Efficiency:	2.5% at 6943$\mathring{A}$
Enclosure and Optical Mount	
Enclosure:	Optical system is mounted to a sturdy alluminum "I" beam and completely enclosed by dust covers. Electronics are contained in two consoles.
Optical Mount:	0-90° elevation angle, manually controlled, 0-360° azimuth angle, motor driven.
Data Display	
Oscilloscope:	Tektronix, type 556, dual channel, 50 MH_z bandwidth
Camera:	Tektronix, Type C-12, 3¼ x 4¼ polaroid film
Data Processing	
Digitizer:	Calma 303, manual curve tracing to magnetic tape
Computer	CDC 3300, data out in normalized relative values of apparent backscatter coefficient vs. range.

Azimuth and Elevation Positioner

The optical system (transmitter and receiver) can be manually positioned to any elevation angle from 0° to 90° and rotated electrically in azimuth from 0° to 360° with the positioner shown in Figure 3. Provisions are made to manually read or electrically transmit position information. The system is leveled by viewing a bull's eye level attached to the positioner while adjusting the lock down pads.

Optical Mount:

A sturdy "I" Beam is used to mount the laser transmitter and optical receiver. The optical system is enclosed by dust covers, with two ports on the front of these covers to enable transmission and reception of light. For safety purposes these ports are covered except during system use, preventing unintentional transmission of laser energy. A port is also provided on the receiver dust cover to view the finder scope used to observe the target area and to facilitate receiver alignment. The receiver axis can be moved ±5° with respect to the I-beam axis to accomplish alighment of the transmitter and receiver beams.

The enclosure was designed to allow the transmitter beam to be transmitted coaxially. This modification will allow studies to be conducted at ranges less than 100 meters.

Optical Receiver

The receiver, which is shown in Figure 4, was constructed by interfacing a Questar field model telescope (89 mm. aperature) and a Pacific Photometric photomultiplier assembly, model 62F, with an adaptor designed by Robert Bartz. The adaptor houses the field stop and narrow band interference filter. The

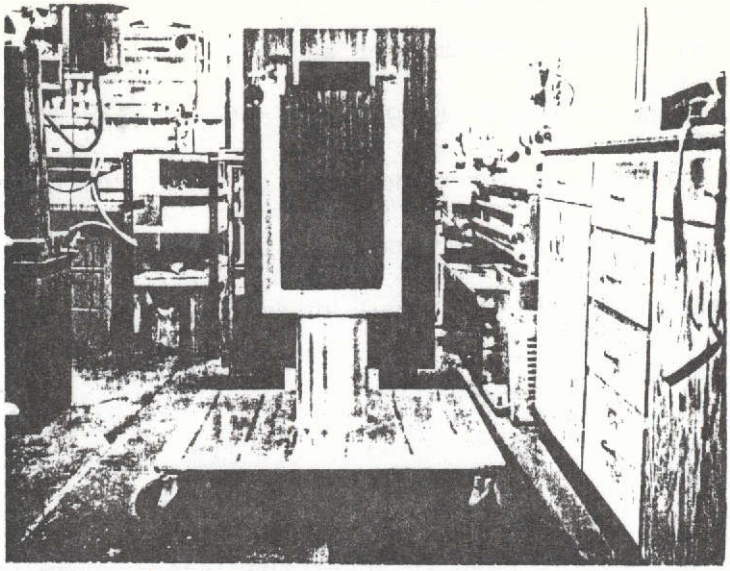

FIGURE 3. AZIMUTH AND ELEVATION POSITIONER WITH "I" BEAM MOUNTED

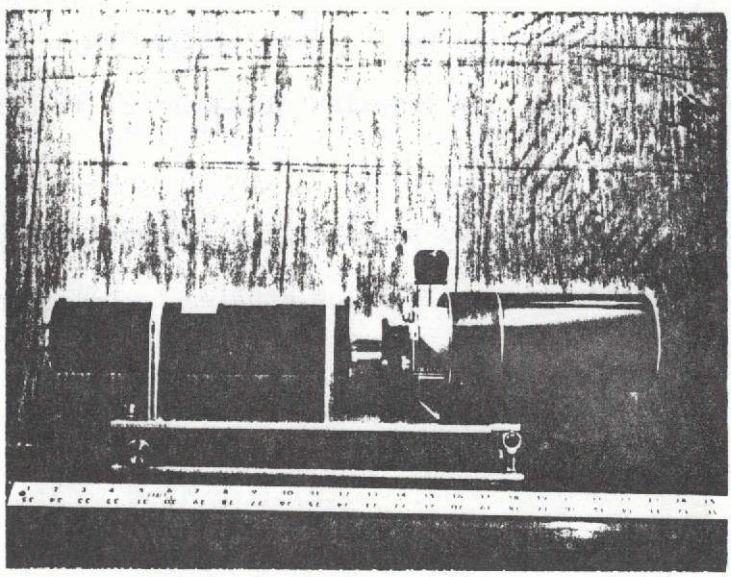

FIGURE 4. OPTICAL RECEIVER

receiver is mounted on a base assembly which permits azimuth and elevation adjustments required for alignment of the receiver and transmitter optical axes. A reticle in the telescope eyepiece is used to align the optical system and to aim it accurately at a known target. The telescope is also equipped with a wide angle finder scope that permits safe operation of the system by enabling the operator to view any obstruction that may come between the system and the intended target. Technical data for the receiver is presented in appendix A.

Laser Transmitter

The transmitter system components, shown in Figure 5 and 6 include a Holobeam Series 300 pulsed ruby laser system (laser head, end mirrors, optical rail, remote station, power supply) a dry Pochels cell Q-switch assembly, and shutter electronics. The Q-switched laser emits radiation at 0.6943 microns with power levels exceeding 100 megawatts. The output power of the laser is monitored through the rear mirror of the laser with a modified Quantronix model 506 power monitor and displayed on one channel of a Tektronix model 556 dual channel oscilloscope.

Electronics

The laser is fired by closing the flash contacts on the oscilloscope camera at a repetition rate determined by the operator. The laser power supply and its safety circuits are contained in the power supply console cabinet. The console operates from a 120 volt 60Hz source. The remote station is connected by a 10-foot multiconductor cable to the power supply. The voltage to which the power supply capacitor bank is charged determines the laser output energy and is preset at the remote station. The energy required to fire the flash lamps to start laser pumping is initially stored in the capacitor bank and then

released through a series inductance upon command from the firing circuit. The laser cooling unit is contained within the power supply cabinet and is accessible through the rear panel door.

The laser Q-switch (Figure 6) consists of the Pockels cell assembly, the shutter electronics power unit, remote control station, and connecting cables. The Pockels cell assembly contains a dry KD*P crystal, a polarizer, and a maximum reflectivity dielectric mirror. At the instant the flashlamp in the laser head is fired, this cell is cross-polarized with respect to the polarized light from the laser rod. In this condition, the cell is off and lasing action is inhibited. After a set delay time (controlled by the Pockels cell remote station), during which the population inversion of excited atoms within the rod rises to extremely high levels, a high-voltage pulse is applied to the crystal. This causes a 90 degree rotation of the plane of polarization of the cell and lasing occurs as a giant pulse of 15-30 nanosecond duration with peak power exceeding 10^8 watts. Before conventional lasing can begin or a second pulse can occur, the voltage applied to the Pockels cell crystal decays and the plane of polarization of the crystal returns to its blocking condition.

Optical Receiver

The field of view of the telescope is limited to five milliradians by a field stop. After passing through the field stop, light collected by the telescope passes through an interference filter with a bandwidth of 10Å to an RCA 7326 photomultiplier tube. Photomultiplier output is buffered by an emitter follower and applied to one channel of the oscilloscope.

Receiver gain is controlled by adjusting the photomultiplier tube supply voltage. Sensitivity and current amplification characteristics of the photomultiplier tube are given in appendix A.

The photomultiplier power supply is a Pacific Photometrics Model 203 high voltage power supply. Power supply voltage can be adjusted from zero to -2000 volts D.C. This power supply also contains a ±15 V.D.C. output that is used to provide voltage to the emitter follower used to buffer the photomultiplier tube output.

Display and Recording

The laser output power and atmospheric backscatter return signal are displayed on separate channels of a Tektronix 556 dual channel oscilloscope. These signals are recorded by photographing the oscilloscope display with a Tektronix C12 oscilloscope camera using polaroid film.

The camera shutter flash contacts, which are controlled remotely by the observer operator, are used to fire the laser system. All controls can be preset to display, record and fire the system which allows one man to operate the lidar system. The data display electronics are shown schematically in Figure 7.

Electronic Calibration

The lidar system is calibrated in range only by means of a Tektronix 181 time mark generator.

Data Reduction

The return signal is displayed on an oscilloscope and photographed with a polaroid camera. Return signal strength and range information will be extracted from the photograph as x, y coordinates by means of a Calma 303 digitizer (available at OSU Computer Center) which stores the coordinates directly on magnetic tape. The x, y coordinates of the photograph and the

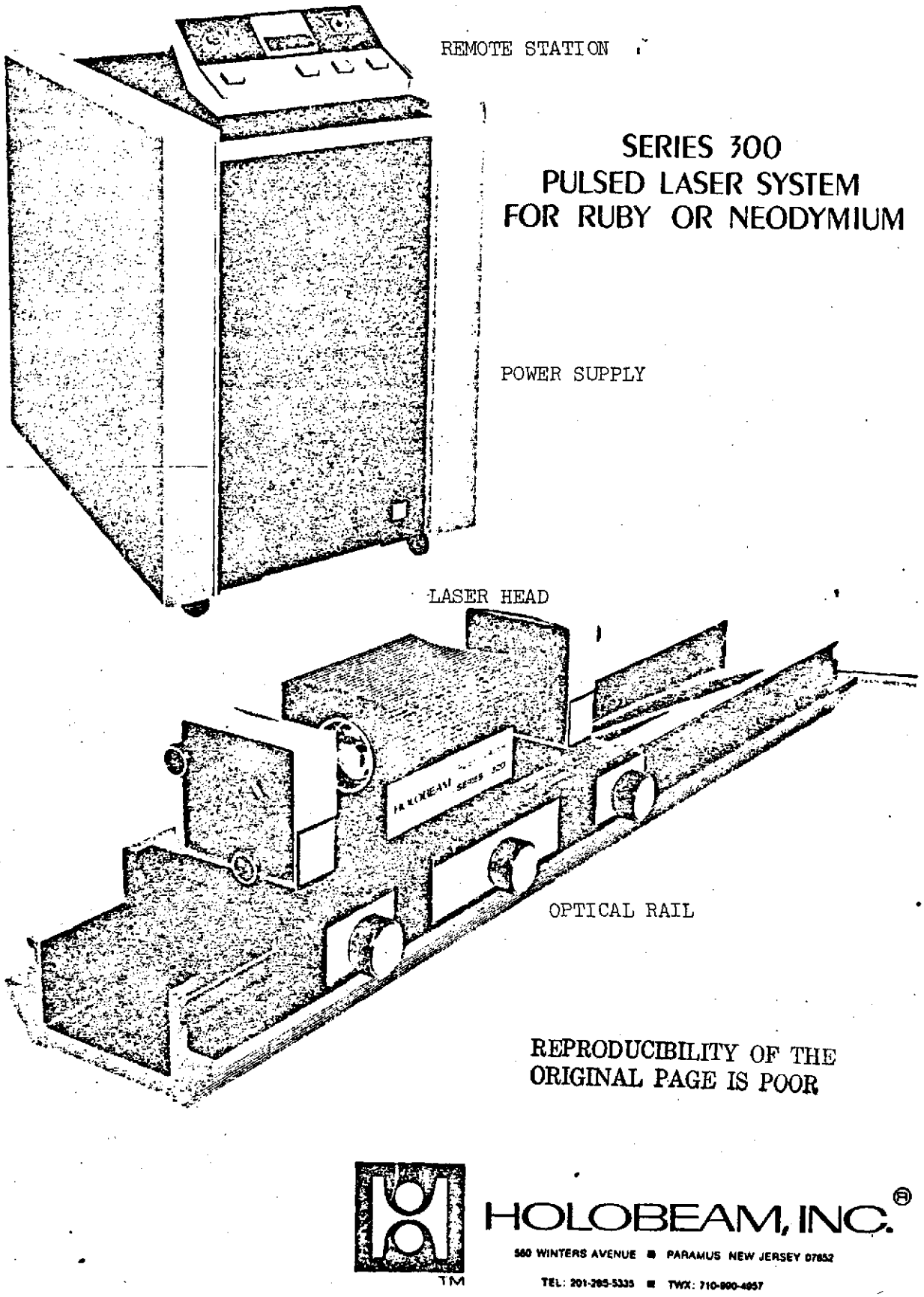

FIGURE 5. HOLOBEAM SERIES 300 PULSED RUBY LASER SYSTEM

SHUTTER ELECTRONICS

POCKELS CELL
LASER Q-SWITCH

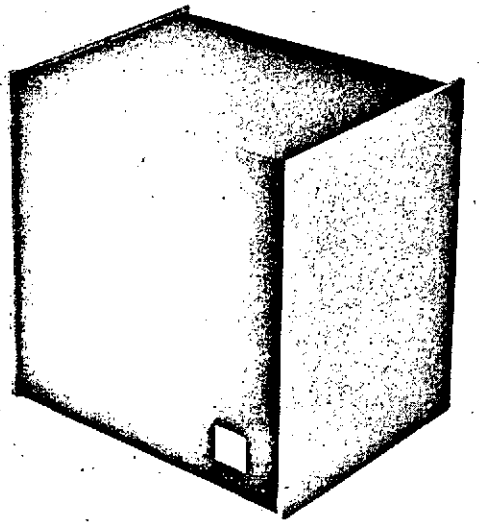

REMOTE
CONTROL
STATION

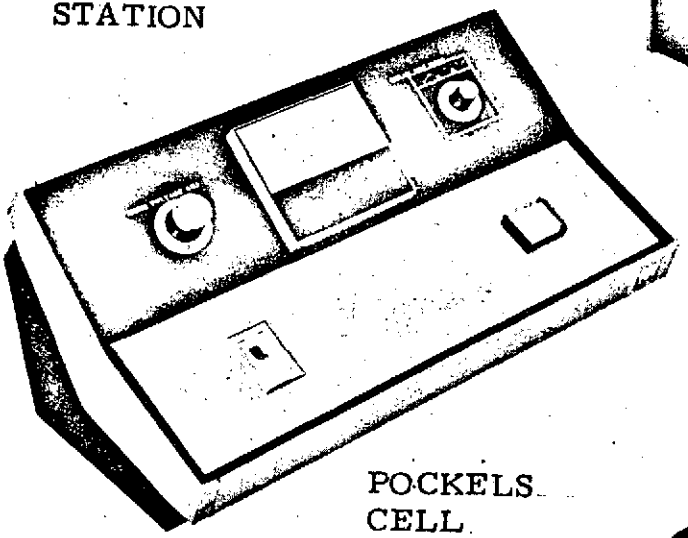

POCKELS
CELL
ASSEMBLY

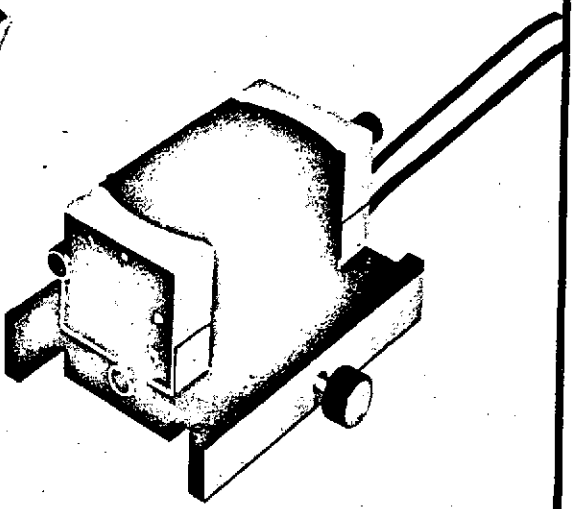

HOLOBEAM, INC.®

560 WINTERS AVENUE ■ PARAMUS NEW JERSEY 07652

TEL: 201-265-5335 ■ TWX: 710-990-4957

TM

FIGURE 6. HOLOBEAM POCKELS CELL Q-SWITCH ACCESSORY

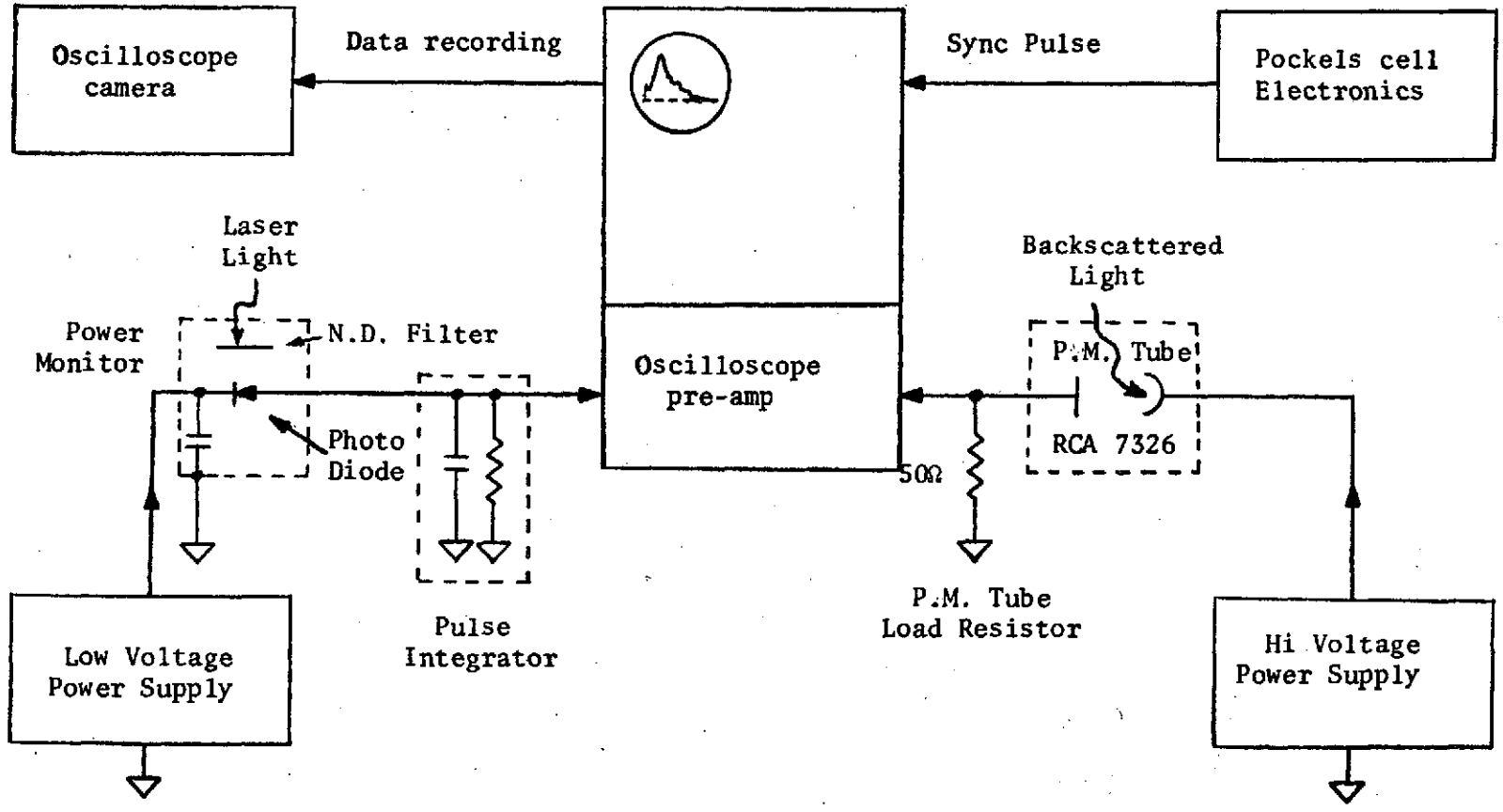

FIGURE 7. DATA DISPLAY ELECTRONICS SCHEMATIC DIAGRAM

required system parameters will then be fed into the OSU CDC 3300 computer. The computer output will consist of range-corrected, normalized, relative values of the apparent backscatter coefficient vs. range. A block diagram of the data reduction scheme is shown in Figure 8.

3. Testing of the System

During August and September of 1972, a special field study to investigate the effect of agricultural field burning on the surface energy budget was undertaken near Corvallis, Oregon. During the period from August 28, 1972 to September 1, 1972, several vertical aerosol profiles were obtained by operating the lidar from a site on the Oregon State University Campus. The vertical aerosol profiles obtained with the lidar system were analyzed and the "actual mixing heights" (defined here as the height at which there is a pronounced decrease in aerosol concentration[1]) were compared with mixing heights estimated from data collected by other means during the above mentioned special field study. Figure 9 shows typical polaroid photographs of the lidar return signal obtained during this period.

Mixing heights obtained from the various observational methods are presented in Table 2. It should be kept in mind that the radiosonde observations were made in Salem, approximately 30 miles north of Corvallis, while the aircraft ascents, pibals winds aloft measurements, and acoustic soundings were made approximately 5 miles south of Corvallis. There is a general agreement between the various simultaneous estimates of mixing height on most occasions. Nevertheless, there are considerable spatial and temporal variations in the estimated mixing heights, a finding in agreement with the results of previous investigations.[1,2,3]

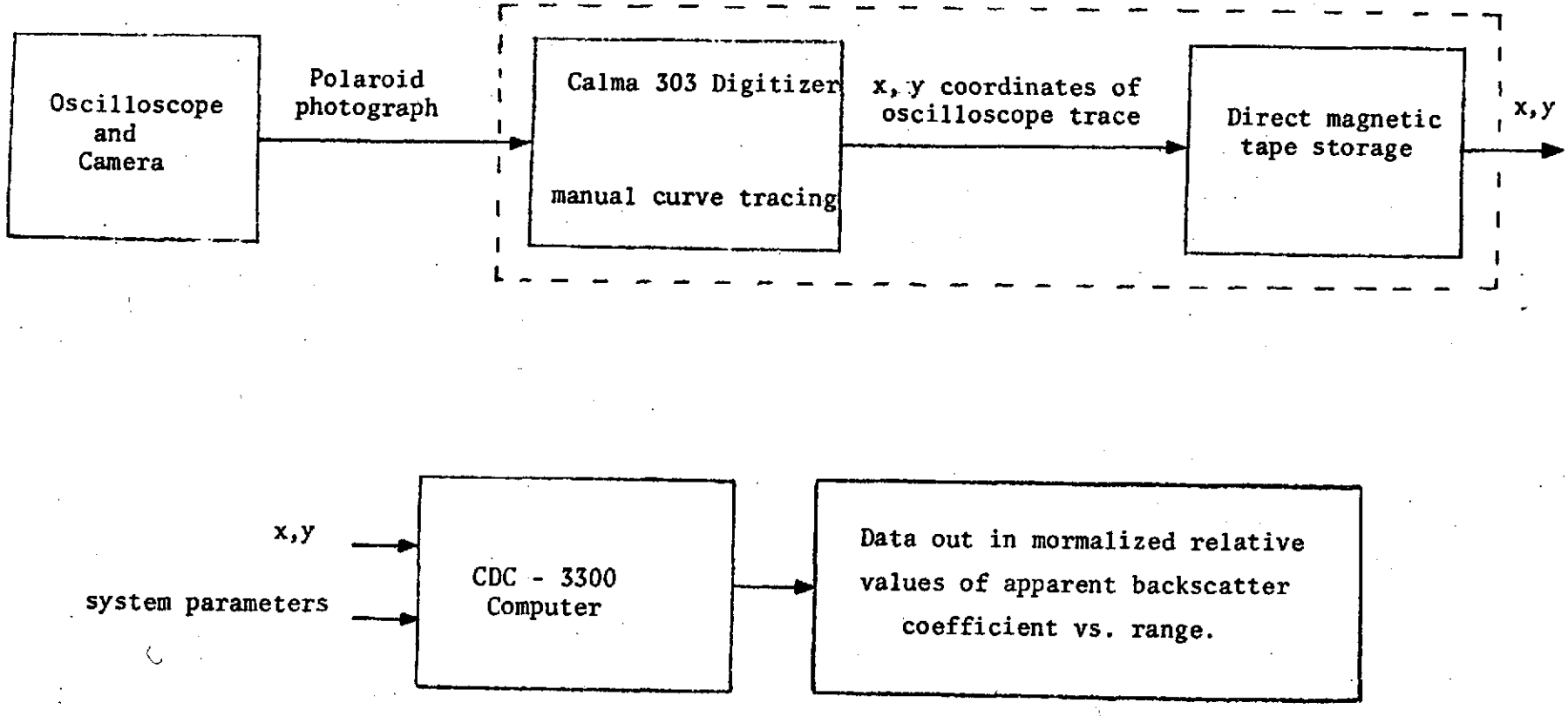

FIGURE 8. DATA REDUCTION SCHEME

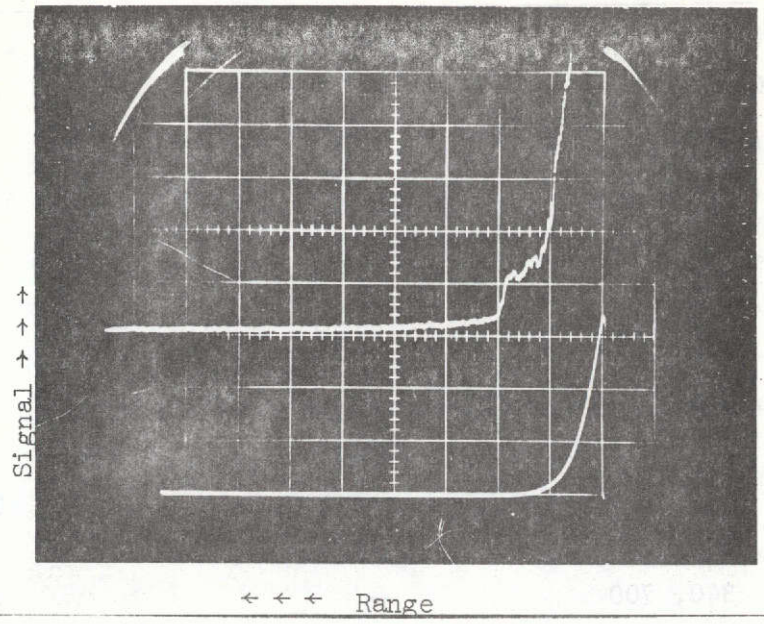

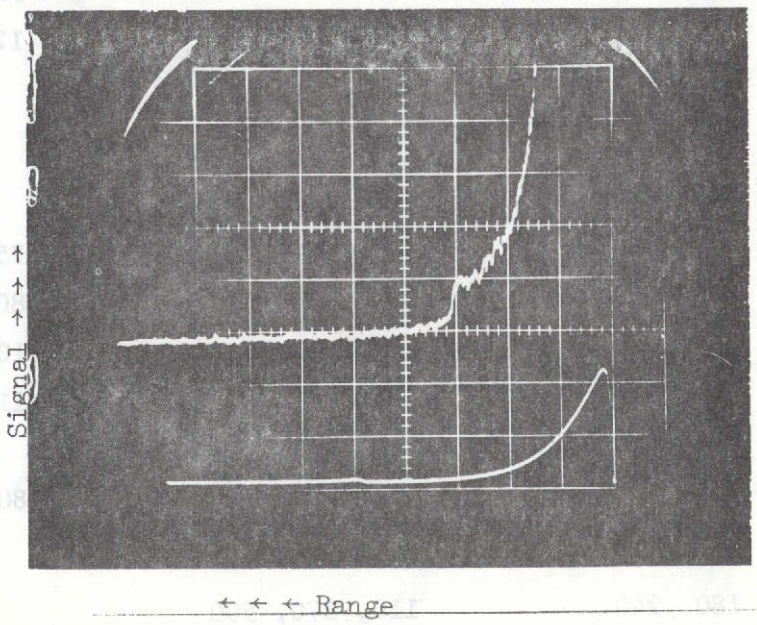

FIGURE 9. TYPICAL LIDAR RETURNS SHOWING TOP OF HAZE LAYER IN WESTERN OREGON, RANGE 375 m/cm

TABLE 2

Mixing Heights (Meters) Estimated by Lidar Compared with Estimates Made by Other Techniques

Sounding Time (LST)		L-R	RAOB	AIRCRAFT	W-S	A-S
8-28	1645	1200	1400	--	1400	--
	1945	1200	--	--	--	
	2010	800, 1200	--	--	--	200
	2400	600, 1100	--	--	1100	200
8-29	0400	270, 600	740			100
	0630	340, 890	--			
	0730	420, 890	--			
	1115	495, 940	--			
	1500	730	1700			700
	1715	600	--		900	250
	1945	370, 670	--			400
	2200	100, 340, 700	--		500	450
	2400	330	--			450
8-30	0400	850 (cloud)	100, 750 2650		1500	200
	0700	340, (670)	--			100, 300
	1000	700	--	700	400, 750	700
	1400	800, 1000	--		990	400*
	1600	890	1250, 2100		1200	400*
	1945	890	--			400*
	2015	270, 670	--			400*
8-31	0400	290, 440, 730	100, 530			150
	0700	760			750	300
	1000	600			800, 900	600
	1330	800			1000	400*
	1600	760	1460		1100	--
	1900	320, 440, 650, 690				--
	2200	310, 730			800	450
	2400	490				500
9-1	0400	130, 180, 240	110, 370, 500			
	0800	440, 730				

*) Where no clear indication of stable layer aloft was seen on the A-S chart the estimated value represents the height of the tops of the thermal plumes.

LR - lidar
RAOB - U.S. National Weather Service Radiosonde
A-S- Acoustic Sounder
W-S- Windshear Layer from Pibal Measurement.

Figure 10 shows the range-corrected lidar signal and the vertical temperature sounding obtained at 1600 PST on August 30, 1972. There is a pronounced decrease in range corrected signal return through a layer near the base of an elevated inversion.

4. Conclusions

The results presented in the preceding section indicate that the optical radar system developed at OSU under NASA Grant No. NGR-38-992-048 meets the design objectives set forth in the Development Plan.[4] Accordingly, the instrument is capable of gathering data on a spatial and temporal resolution that is impossible or infeasible with most other techniques. This capability enables one to construct a detailed picture of atmospheric structure which may furnish valuable insight into the nature of some atmospheric porcesses.

5. Suggested Equipment Modifications

The following modifications and additions to the instrument system are suggested:

1. The data display system should be converted from oscilloscope polaroid photography to a real time display that presents in raster or map form the spatial and/or temporal distribution of backscatter profiles. This would make possible RHI, PPI and time-height cross section type displays.
2. The data recording system should be converted from oscilloscope polaroid photography to a fast analog to digital converter that samples and digitizes the return signal. Integrated circuits that are fast enough for this purpose are commercially available. Once the signal has been sampled and held in digital form, it could be immediately analyzed with a small on-line computer and stored on a magnetic disc recorder for instant replay in the display type of

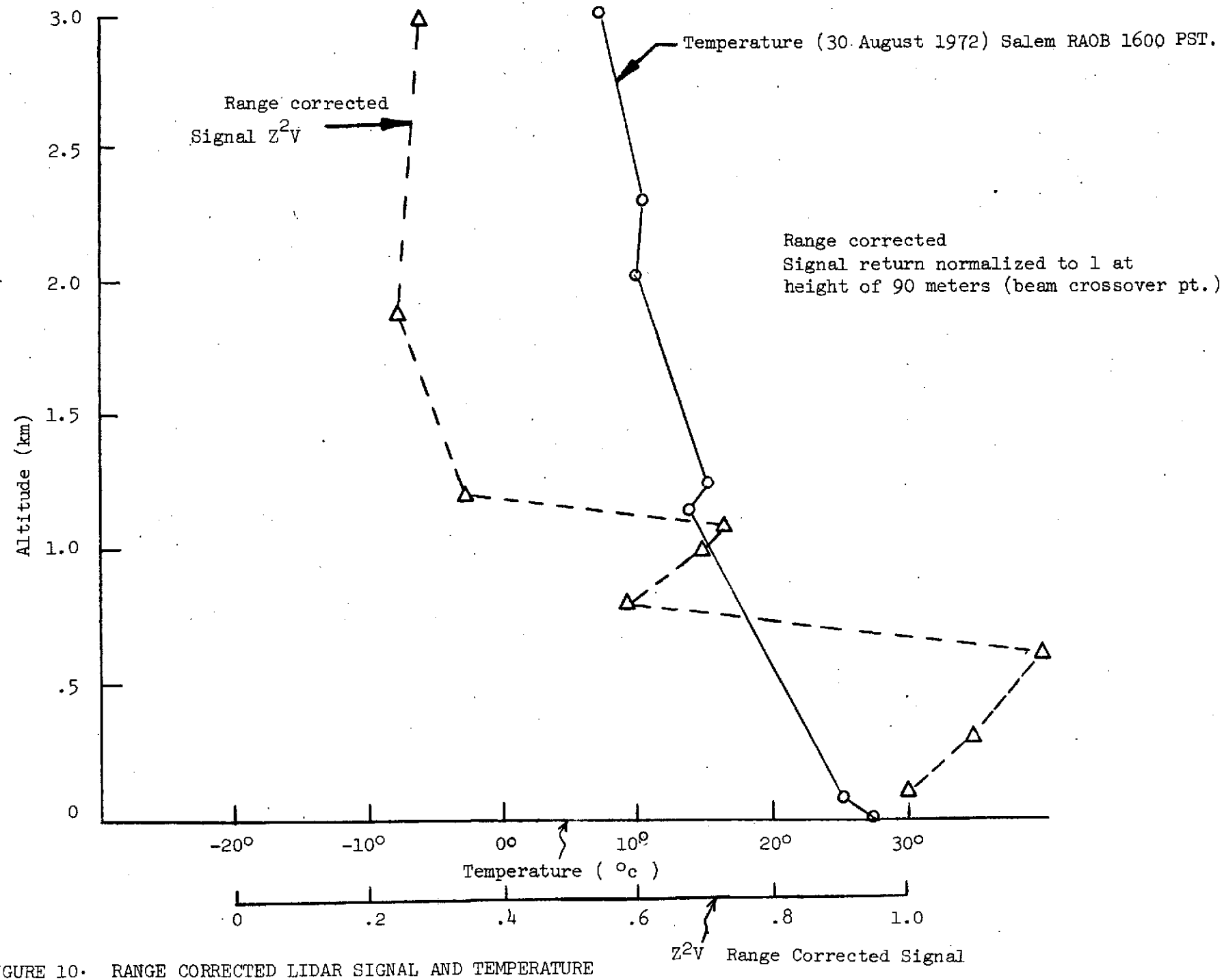

FIGURE 10. RANGE CORRECTED LIDAR SIGNAL AND TEMPERATURE VERSUS ALTITUDE FOR 1600 PST, 30 AUGUST 1972.

the operator's choice.

3. The system should be made mobile by mounting it in a small truck equipped with its own power supply and air conditioning equipment.

4. The transmitter and receiver optics should be made coaxial to permit measurement of signal returns from target volumes located at distances less than about 150 meters from the instrument.

These modifications would significantly enhance the present capability by permitting mobile operation, observation of the close-in return, on the spot inspection of the atmospheric area being surveyed, and real time data analysis. It has not been the purpose of this section to describe in detail the electronic and mechanical constructs necessary for these modifications. Allen and Evans[5] have reported details of a recently developed system that incorporates most of these modifications.

6. Suggestions for Future Research

Although the development of an active observational research program involving the optical radar system has been delayed by lack of funds, the following uses for the instrument have been seriously considered:

1) Observations of the spatial and temporal variations of the mixing height related to the influence of topographical inhomogenities on wind fields and surface heating, dynamic and thermodynamic influences of local wind systems, radiative effects of polluted layers, and urban heat island effects.

2) Observations of the changes in the stratification and transport of suspended particulate matter during the development of mesoscale thermal-tidal wind systems.

3) Observations of plume behavior and diffusion in mountainous terrain with particular emphasis on the behavior of a plume approaching an obstacle such as a butte or a bluff.

4) Observations of sea-salt spray generation in the coastal surf zone.

7. References

1. McCormick, M. Patrick, S. Harvey Melfi, Lars E. Olsson, Wesley L. Tuft, William P. Elliott, and Richard Egami, 1972. Mixing Height Measurement by Lidar, Particle Counter, and Rawindsonde in the Willamette Valley, Oregon, NASA TN D-7103, National Aeronautics and Space Administration, Washington, D.C., December 1972; 78 pp.

2. Olsson, L.E. and W.L. Tuft, 1971. A study of the Natural Ventilation of the Columbia-Willamette Valleys: II. Tech. Report #71-2. Dept. of Atmospheric Sciences, Oregon State University, April 1971; 164 pp + appendices.

3. McCaldin, R.O. and R.S. Sholtes, 1970. Mixing Height Determinations by Means of an Instrumented Aircraft. Engineering and Industrial Experiment Station, College of Engineering, University of Florida. Gainsville, Fla., June 1970; 30 pp.

4. Bartz, Robert and Charles Craig, 1971. Development Plan for the Optical Radar System under NASA Grant # NGR-38-992-048. Submitted to NASA in 1971.

5. Allen, R.J. and W.E. Evans, 1972. Laser Radar (LIDAR) for Mapping Aerosol Structure. Review of Scientific Instruments, 43, 14422-1432.

8. Appendixes

Appendix A Optical Receiver Technical Data

Appendix B Laser System Technical Data

Appendix C Lidar Range Equation and Computer Programs for its Solution

Appendix D Miscellaneous System Photographs

APPENDIX A

OPTICAL RECEIVER TECHNICAL DATA

QUESTAR SPECIFICATIONS

TYPE: Maksutov Cassegrain Catadioptric. No coma, astigmatism or spherical aberrations.
CLEAR APERTURE, 3.5 inches, 89 mm.
FOCAL LENGTH, Basic Visual, 50.5 inches, f/14.4, 1300 mm.
FOCAL LENGTH, Camera Close, 56 inches, f/16, 1400 mm.
FOCAL LENGTH, Camera with Ext. Tubes, 64 inches, f/18, 1600 mm.
FINDER LENS, 4" Fl., 4x and 8x, Field 12° and 8°.
POWERS, 40–80x eyepiece, field 55 min.
POWERS, 80–160x eyepiece, field 42 min.
POWERS LIMIT: Resolves 1 sec. arc at 50 feet EFL.
FIELD OF VIEW, photographic model, 1°30 min.
EYEPIECES, 26mm. Koenig, 50°Ap. Field; 12 mm. 5-lens Erfle, 75°Ap. Field.
AMPLIFYING OR BARLOW LENS, minus 43.9 mm. FL.
ERECTING PRISM, Star Diagonal type, 90°.
STANDARD SUN FILTER, 1-1/2" aperture glass flat, off-axis mount with exact measured thickness of chromium coating allowing a .002% to .003% light transmission.
FULL-APERTURE SUN FILTER, 3-1/2" clear aperture, exact measured thickness of chromium coating allowing a .002% to .003% light transmission.

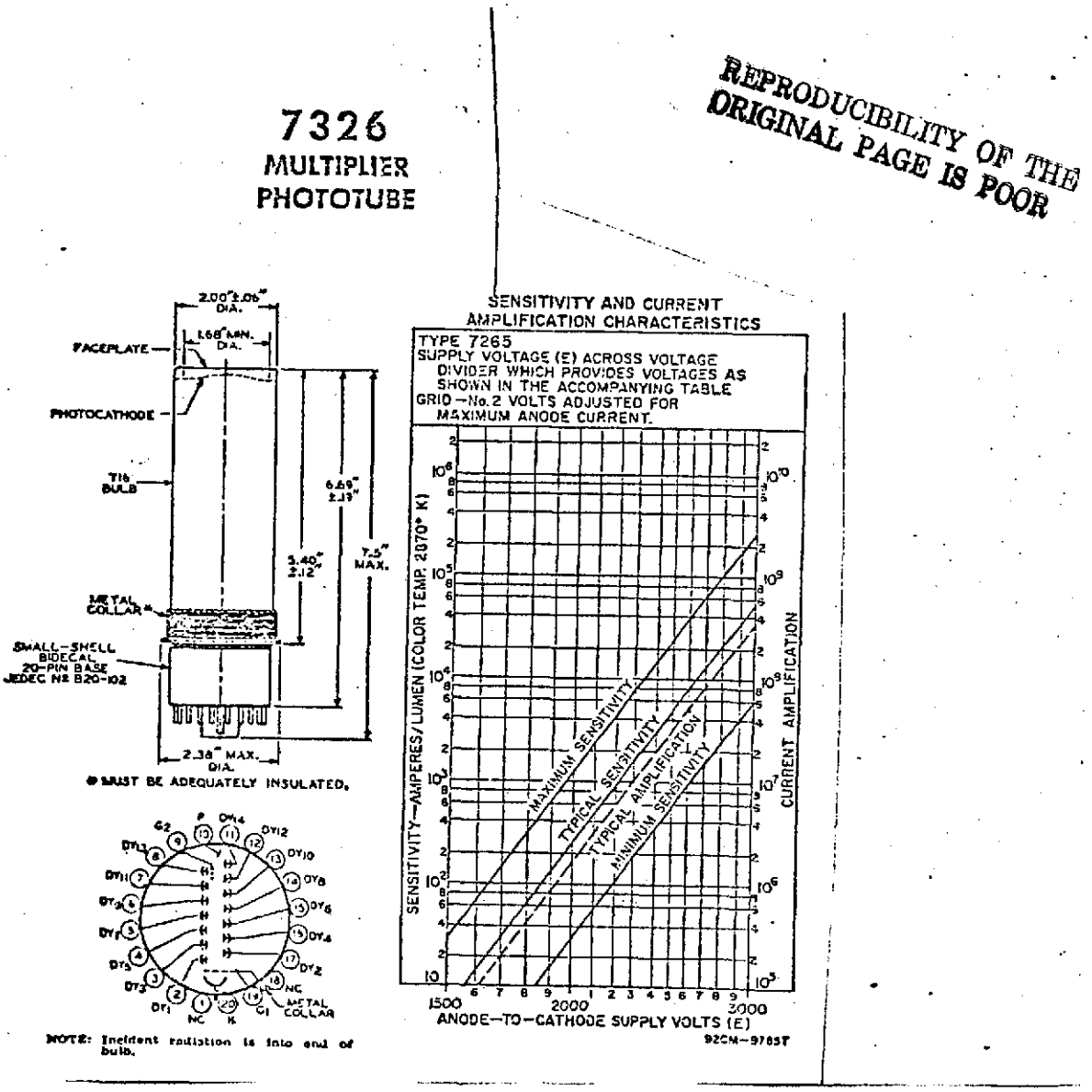

Figure A-1

Multiplier Phototube

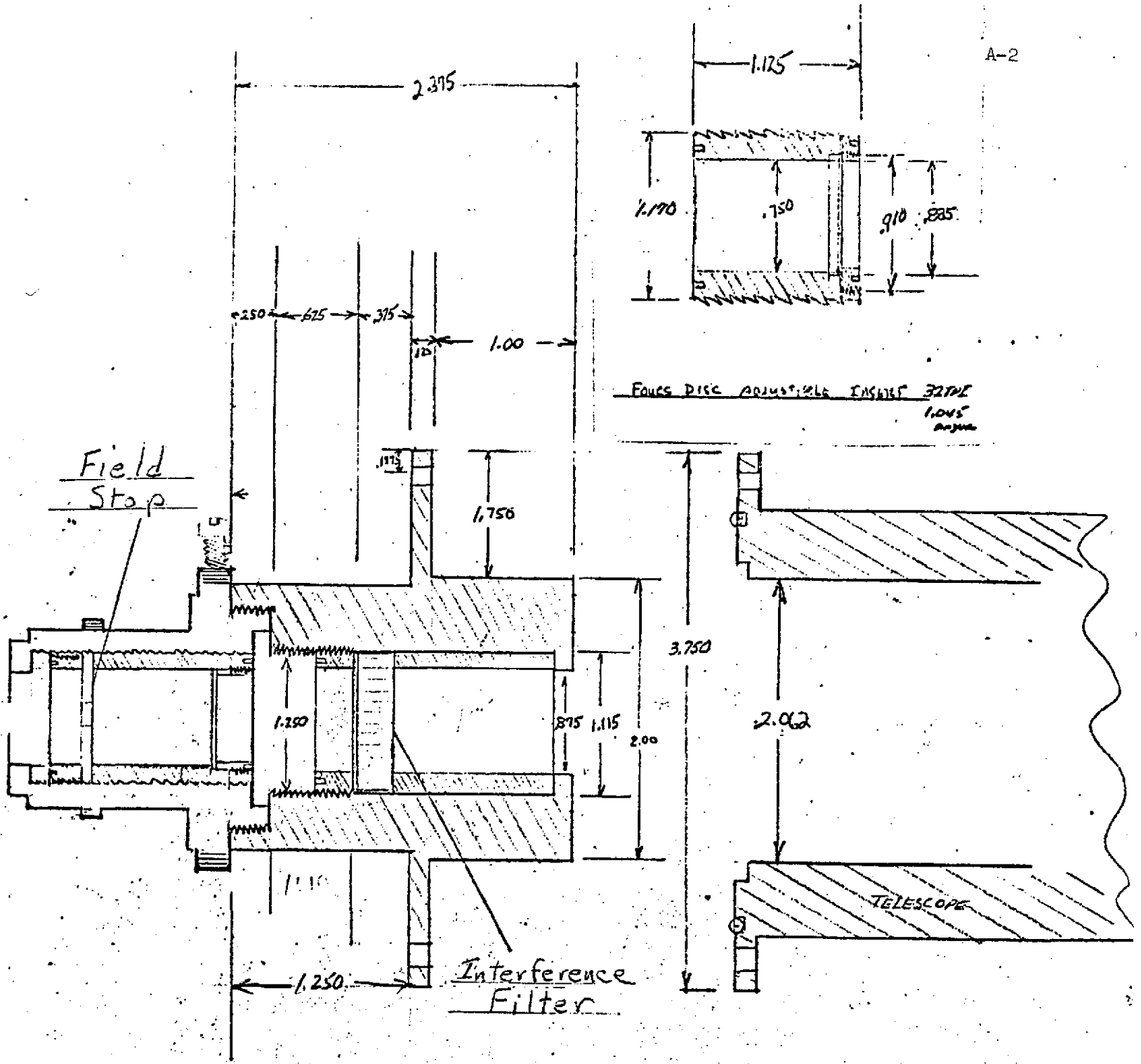

Figure A-2

Telescope P.M. Tube Adaptor

7539692	Northwest Precision Products 439 S. W. 2nd Street Corvallis, Oregon 97330
SCALE: 1" = 1"	APPROVED BY
DATE: 12-31-71	R. BARTZ
P.M. TUBE ADAPTOR - TELESCOPE	

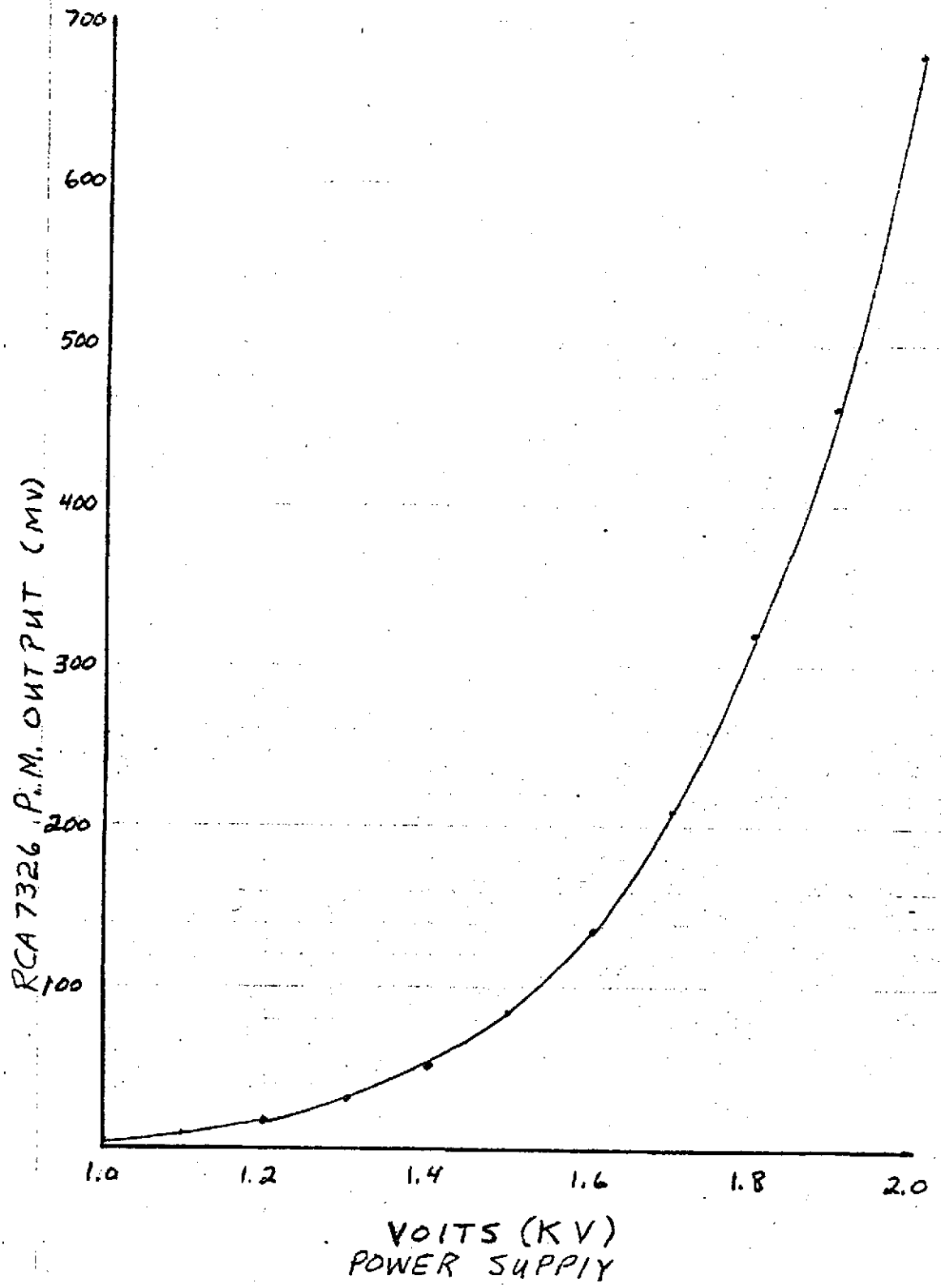

Fig. A-3 Relative P.M. TUBE GAIN VS POWER SUPPIY VOITAGE

APPENDIX B

LASER SYSTEM TECHNICAL DATA

TECHNICAL DATA SHEET

SERIES 300 WITH POCKELS CELL Q-SWITCH ACCESSORY

CUSTOMER OREGON STATE UNIVERSITY

HOLOBEAM JOB NO. 284000

SHIP BY _____

LASER SYSTEM DATA

LASER ROD 3" X 3/8" RUBY SER.# Q-74

REAR REFLECTOR MAX. R. @ 6943Å RADIUS CURV. = ∞

OUTPUT REFLECTOR 25% R. @ 6943Å RADIUS CURV. = ∞

POCKELS CELL CRYSTAL KD*P

POWER SUPPLY 5KV VARIABLE

CAPACITOR BANK 220 μF

PARAMETER	SPECIFICATION REQUIRED		MEASURED	
LASING THRESHOLD	N.A.	KV	3.05	KV
OUTPUT ENERGY	1.5	Joules	2.17	Joules @ 3.60 KV
PULSE WIDTH	15-30	nsec	20	nsec @ 3.60 KV
PEAK POWER	100	MW	108	MW @ 3.60 KV
LINE WIDTH	N.A.	Å	N.A.	Å
BEAM DIVERGENCE (FULL WIDTH, ½ POWER)	3-5	MRAD	3.8	MRAD
POCKELS CELL VOLTAGE	N.A.	KV	8.0	KV
POCKELS CELL DELAY	N.A.	usec	1000	usec

Roach Isley — ENGR TEST — 3/7/72 DATE

Q.C. — 3/7/72 DATE

NOTE: DATA TAKEN WITH WATER TEMP. CONTROLLED AT 30.0°C

TECHNICAL DATA SHEET

SERIES 300 WITH POCKELS CELL Q-SWITCH ACCESSORY

HOLOBEAM JOB NO. 284000

A. REMOTE STATION DELAY SETTING

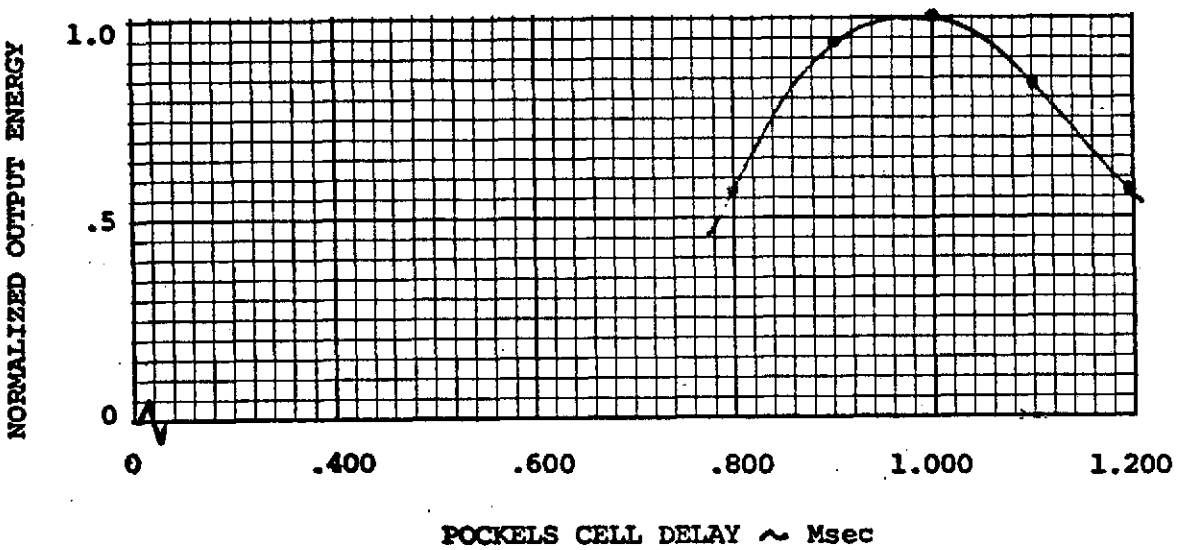

B. REMOTE STATION VOLTAGE SETTING

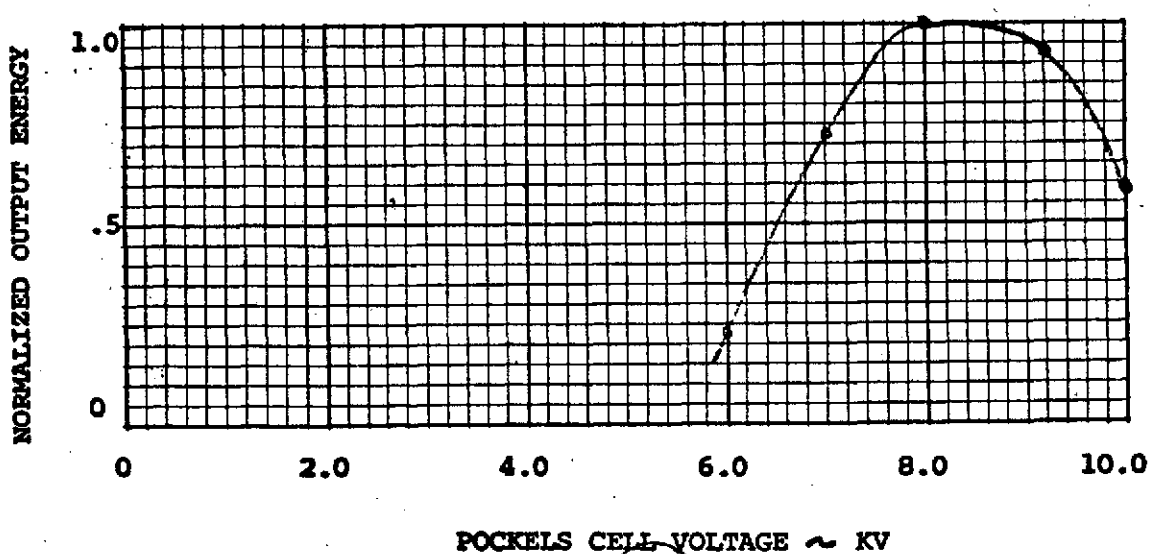

Joseph Lotz 3/7/72
ENG. TEST DATE

Q.C. 3/7/72
DATE

TECHNICAL DATA SHEET

C. NORMALIZED OUTPUT POWER

NORMALIZED TO 108 MW.

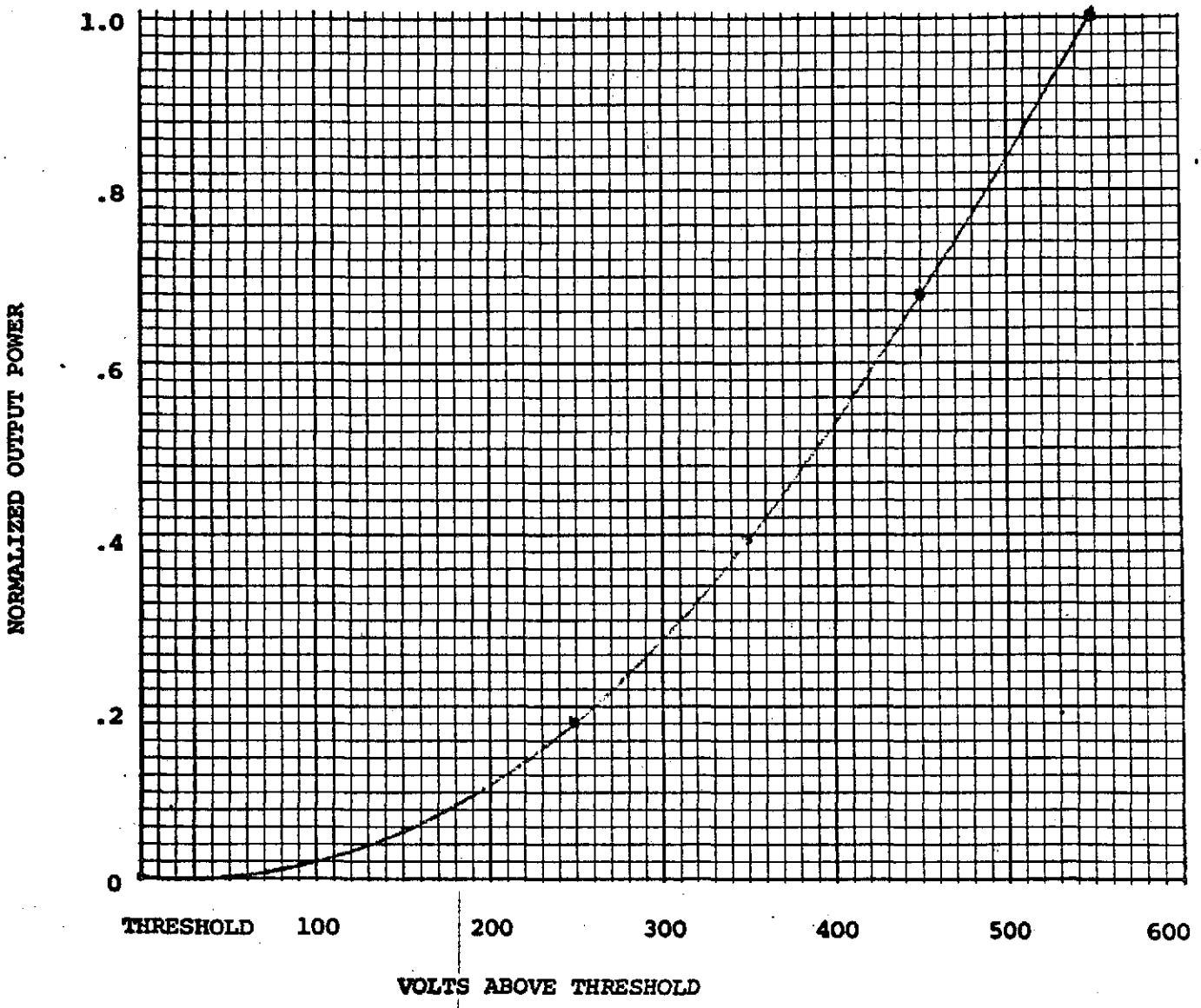

ENG. TEST — DATE 3/7/72

Q.C. (212) — DATE 3/7/72

APPENDIX C

THE LIDAR RANGE EQUATION AND COMPUTER PROGRAMS FOR ITS SOLUTION

The following text and computer programs were supplied by Dr. G.W. Bethke, Space Sciences Lab., General Electric Company, P.O. Box 8555, Philadelphia, PA 19101, and are reproduced verbatim.

APPENDIX A

THE LIDAR RANGE EQUATION AND COMPUTER PROGRAMS FOR ITS SOLUTION

I. Range Equation Derivation

It is assumed that the laser light source is pulsed, with light pulses which are short in length compared to the measurement ranges of interest. It is also assumed that the laser beam is collimated to a divergence which is smaller than the lidar receiving system angle of acceptance (field of view). It is further assumed that the transmitted laser beam is coaxial or nearly coaxial with the receiving system, such that the propagating laser beam is located entirely within the receiving system field of view during the period (ranges) of interest. Because the laser beam is located entirely within the receiver field of view, only the total power (P_L) and energy (E) of the laser beam need be considered, and not the beam intensity.

The total power of incident light (P_i) scattered in direction θ by illuminated scattering length (ℓ) of gas is

$$P_s(\theta) = P_i \ell \cdot k_s(\theta) \qquad (1)$$

where $k_s(\theta)$ is the directional scattering coefficient.

Now referring to Figure A-1, we see that a pulse of light which starts from the laser at time t_o and continues to be emitted until time t_L, has a length L, where

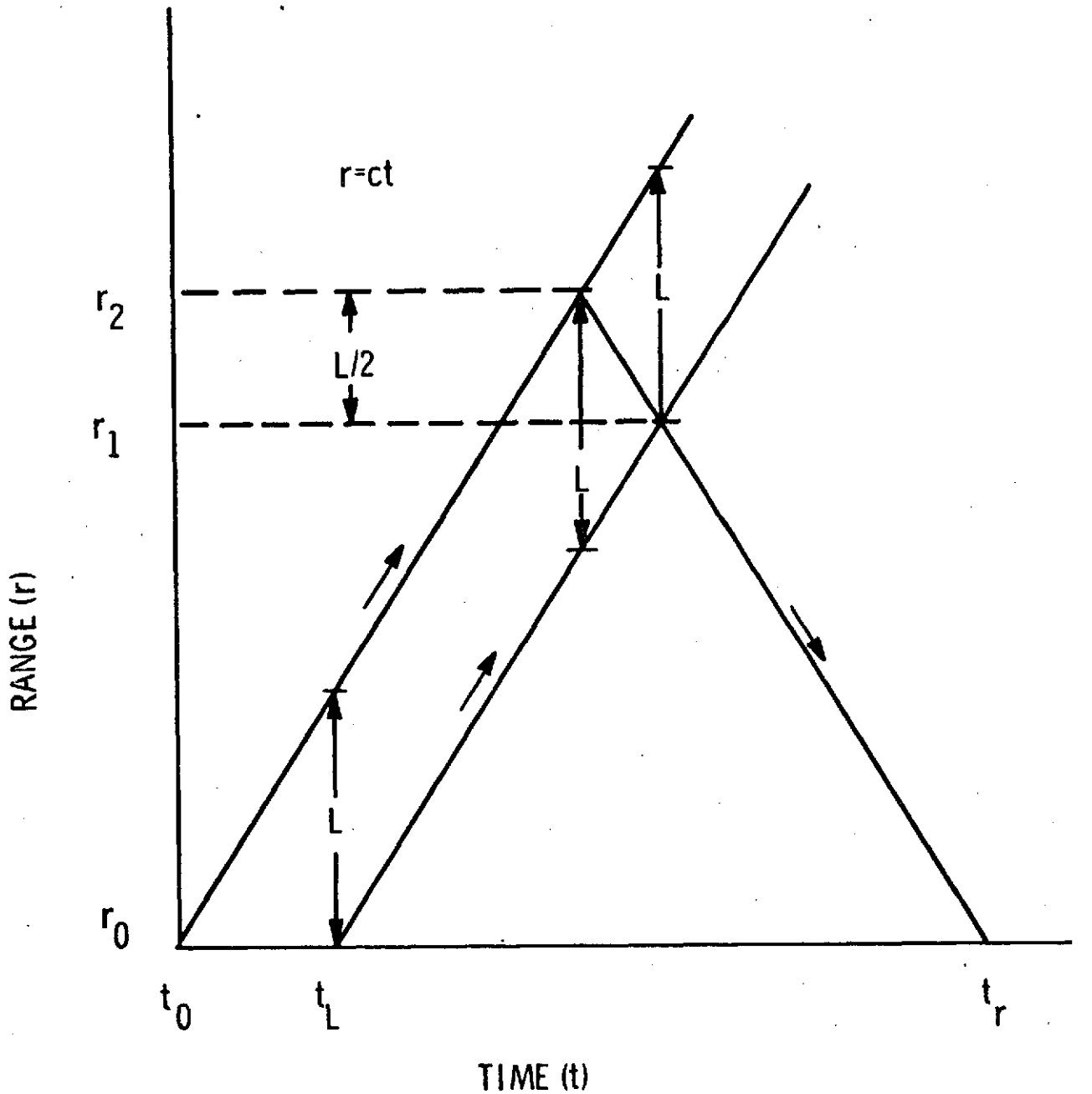

Figure A-1. Laser pulse range vs. time diagram. This diagram illustrates the length (L/2) of the lidar system laser pulse scattering volume which is observed at time t_r, for a laser pulse of length L.

$$L = c\,(t_L - t_o) = c\,t_L \qquad (2)$$

As this short light beam of length L propagates away, light is continuously scattered back to the lidar system. However, Figure A-1 illustrates that the scattered light observed by the lidar system at any one instant in time, t_r, is scattered only from incident light located between ranges r_1 and r_2 which have a distance difference of L/2. Thus the illuminated length of gas that scatters light back towards the lidar system at any one time, t_r, is

$$\ell = r_2 - r_1 = L/2. \qquad (3)$$

The light which left the lidar laser with power P_L arrives at the range of interest (r) with reduced incident power P_i due to atmospheric extinction. Thus

$$P_i = P_L \exp(-r k_e) \qquad (4)$$

where k_e is the total extinction coefficient of air from all sources assuming extinction to be constant with range. Finally,

$$P_L = \dot{E} = E/t_L \qquad (5)$$

where E is the total laser energy per pulse. Now combining equations 1 through 5, we have

$$P_s(\theta) = (cE \cdot k_s(\theta)/2) \exp(-r k_e). \qquad (6)$$

The power of back-scattered light collected (P_c) by the lidar receiving objective is

$$P_c = P_s(180^\circ) \cdot \Gamma \exp(-r k_e) \qquad (7)$$

where Γ is the solid angle subtended by the lidar receiving objective from the scattering range r. But

$$\Gamma = 2\pi(1 - \cos\gamma) \approx \pi\gamma^2 \approx A/r^2 \qquad (8)$$

where γ is the angle subtended by the radius of the lidar receiving objective from scattering distance r, and A is the area of the receiving objective. Since it has been assumed that the light pulse is short in length compared to the measurement ranges of interest, we can assume with negligible error that Γ is the same at any one instant (t_r) from all portions of the illuminated scattering volume. Finally, the power of scattered light which reaches the detector (P_d) is

$$P_d = E_o P_c \qquad (9)$$

where E_o is the total efficiency of all optics in both the transmitting and receiving sections of the lidar system. Thus combining equations 6 through 9 we have

$$P_d = \frac{c}{2} \frac{A}{r^2} E_o E k_s(180^\circ) \cdot \exp(-2r k_e) . \qquad (10)$$

If P_d is in watts and the detector has a sensitivity S in amps/watt, then the voltage drop, V, produced by detector output current I across detector load resistor R is

$$V = IR = P_d S R \qquad (11)$$

The directional scattering coefficient consists of both molecular (Rayleigh) scattering, and particulate or aerosol (Mie) scattering.

$$k_s(\theta) = n(r) \cdot \sigma_R(\theta) + C_1 m(r) \cdot \sigma_M(\theta) \qquad (12)$$

Here, n is the molecular concentration (density) in air, $\sigma_R(\theta)$ is the directional Rayleigh cross section, m is the particulate concentration in air, $\sigma_M(\theta)$ is the suitably size-integrated directional Mie theory-calculated cross section for particulates in the air, and C_1 is a factor which corrects the Mie theory-calculated $\sigma_M(\theta)$ to the correct value for the real atmospheric aerosol. Similarly, the total extinction coefficient is defined as molecular (Rayleigh) and particulate or aerosol (Mie) total scattering plus any molecular absorption at the specific wavelength of interest.

$$k_e = n(r) \cdot \sigma_R + C_2\, m(r) \cdot \sigma_M + k_a \qquad (13)$$

Here σ_R is the total Rayleigh cross section, k_a is the absorption coefficient of air at the laser wavelength, σ_M is the total Mie theory-calculated cross section, and C_2 is a factor which corrects the Mie theory-calculated σ_M to the correct value for the atmospheric aerosol. As is clear from equation 13, k_e is not constant with range. Consequently, we must replace the expression $(r\,k_e)$ in equations 4, 6, 7, and 10 with

$$r\,k_e \rightarrow \sigma_R \int_o^r n(r)dr + C_2\,\sigma_M \int_o^r m(r)dr + r\,k_a\,. \qquad (14)$$

Finally, combining equations 10, 11, 12, and 14, one obtains the range equation

$$V = cR\,SE_o \frac{EA}{2r^2}\left[n(r) \cdot \sigma_R(180^\circ) + C_1\, m(r) \cdot \sigma_M(180^\circ)\right] \cdot \exp - 2\left[\sigma_R \int_o^r n(r)dr + C_2\sigma_M \int_o^r m(r)dr\right]. \qquad (15)$$

Here we have dropped the absorption coefficient of equation 14 because

we assume that the laser wavelength does not coincide with a significant atmospheric line or continuum.

The atmospheric density, n can be expressed analytically if one curve-fits to a suitable standard atmosphere. For lidar system elevations that do not cover a range of more than a few thousand feet above sea level, the following expression is useful to about 50,000 feet scattering altitude:

$$n = n_o \frac{T_o p}{T p_o} \cdot \left[\exp\left(-2.3026 \frac{r}{Z'} \sin\varphi\right) - Z'' r^2 \sin^2\varphi\right] \qquad (16)$$

Here, n_o is the value of n at temperature T_o and pressure p_o, while T is air temperature and p is air pressure near the lidar system, φ is the lidar system angle of elevation above horizontal, and Z' and Z'' are suitable constants. If the lidar system is at sea level and r is in cm, then setting $Z' = 2.31 \times 10^6$ cm and $Z'' = 3.0 \times 10^{-14}$ cm^{-2} gives n values which agree with the AFCRL 1959 standard atmosphere to within $\leq 0.6\%$ and $< 3\%$ at $\leq 30,000$ feet and $\leq 50,000$ feet altitudes above the lidar, respectively. If the lidar system is at 2000 feet altitude, then the same assumptions give agreement to within $\leq 1\%$ and $< 6\%$ at $\leq 20,000$ feet and $\leq 50,000$ feet altitudes above the lidar, respectively. Of course for $\phi << 90^o$, one is not concerned with such high altitudes even when r is large.

II. Computer Solution of the Range Equation

As has been pointed out in section I of this appendix, for the general case of non-constant m(r), the range equation is an integral equation requiring a numerical rather than analytical solution technique. For purposes of clarity in this discussion, the range equation (see equation 15) is reproduced here in a form and notation which are consistent with that used in writing the computer program. It is assumed that $C_1 = C_2 = C \equiv C'$.

$$V = \frac{K}{r^2} \left[C' \sigma_M(180^\circ) \cdot m + \sigma_R(180^\circ) \cdot n \right] \cdot \exp\left(-2 \sigma_R \int_o^r n \, dr - 2C' \sigma_M \int_o^r m \, dr\right) \qquad (17)$$

where

$$K = (1/2) R \, SE_o \, c \, AE$$

and

$$n = x_1 \left[x_2 r^2 + \exp(x_3 r)\right]$$

with

$$x_1 \equiv n_o T_o p/(T p_o) > 0$$

$$x_2 \equiv -Z'' \sin^2 \varphi < 0$$

$$x_3 \equiv -(2.3026 \sin \varphi)/Z'$$

Performing the integration of n with respect to r, one can rearrange equation (17) into the following form:

$$y_1 \exp(y_2) = (m + y_3) \exp\left(y_4 \int_o^r m dr\right) \qquad (18)$$

where

$$y_1 \equiv Vr^2 / [KC'\sigma_M(180^\circ)]$$

$$y_2 \equiv 2\sigma_R x_1 [(x_2 r^3/3) + (1/x_3) \exp(x_3 r - 1)]$$

$$y_3 \equiv \sigma_R(180^\circ) \cdot n / [C' \cdot \sigma_M(180^\circ)]$$

$$y_4 \equiv -2C'\sigma_M \quad .$$

In practice the data points used for the computer solution of equation (17) are V_i and r_i, $1 \leq i \leq 200$ with no restriction on the interval size other than the physically sensible one of taking fine intervals where V varies rapidly. Here, $r_o \equiv 0$, and V_o is unknown and not necessary for solution.

The method of solution for equation (18) assumes $m_o = m_1 =$ constant for the range r_o to r_1. This then gives

$$\int_o^{r_1} m \, dr = m_1 \cdot (r_1 - r_o) \equiv S_1$$

and allows equation (18) which is trancendental in m to be solved iteratively for m by Newton's method, reference (1). Two values of m_1 will satisfy this equation for a large range of values of the physical quantities involved. Only one of the values of m_1 will be correct and will lead to the correct values for m_i for all i. The existence of these two solutions can be explained best from a physical viewpoint. If one considers receiving a backscattered lidar signal from close range (r_1), its level can be relatively small for one of two possible reasons; (a) either m_1 is small, or (b) m_1 through m_o is large, resulting in significant attenuation for range r_1. The first solution (smaller m_1) has been found to be the

correct one for $m_1 \leq 10^4$ μgm/m^3 with $r_1 \leq 4 \times 10^4$ cm, both of these values being much larger than normally encountered in use of the lidar system. Therefore, unless the physical situation (such as dense fog) dictates otherwise, the first solution is selected, although the second solution (if it exists) can be examined readily by using a simple program instruction.

The remainder of the m_i are obtained by successively using the previously calculated values of m_i to evaluate the exponential term in equation (18) in the following manner:

$$\int_o^{r_i} m\,dr = S_{i-1} + \left[(m_{i-1} + m_i)/2\right] \cdot \left[r_i - r_{i-1}\right]$$
$$\equiv S_i \qquad (i > 1) \tag{19}$$

Physically, this has the effect of using the average value of m(r) over the interval in computing this term. Combining equations (18) and (19), one obtains the final form of the range equation as treated by the computer program in solving iteratively at each r_i $(i > 1)$ for m_i using Newton's method.

$$(m_i + y_3) \exp\left[y_4 (r_i - r_{i-1})\, m_i /2\right]$$
$$= y_1 \exp\left\{y_2 - y_4 \left[S_{i-1} + (r_i - r_{i-1})\, m_{i-1} /2\right]\right\} \tag{20}$$

The computer program for performing this solution to the range equation is called RANGM and has been written in Fortran for desk side terminal service to the General Electric 605 computer. The RANGM

program requires the following inputs with the units indicated in parentheses: R (ohms), SE_o (amps/watt), A (cm^2), E (joules), $\sigma_M(180^\circ)$ ($cm^2/(\mu gm\ sr)$), T ($^\circ R$), p(inches Hg), Z' (cm), φ(degrees), Z"(cm^{-2}), C (unitless), σ_M($cm^2/\mu gm$), number of data points, and the data input r (cm) and V (volts). For each input point, the program then prints out r (cm), V (volts), and m ($\mu gm/cc$). A complete listing of this program is shown below.

```
READY
%LIST RANGM                    RANGM

01/13/70   17.370

00010        DIMENSION V(200),R(200)
00020        REAL N0,M,K,MP,MPP
00030        ASCII MSG1,MSG2,MSG3,MSG4,FILE,FIRST
00035        CALL SETERR(15)
00040        MSG1="ERR1"
00050        MSG2="ERR2"
00060        MSG3="ERR3"
00070        MSG4="ERR4"
00080        C=2.9971E+10
00090        SGR=1.6692E-27
00100        SGRT=1.9925E-28
00110        N0=2.6871E+19
00120        T0=491.7
00130        P0=29.921
00140        PRINT:"R,SE0,A,E,SGM,SGMT";READ:CAPR,SE0,A,E,SGM,SGMT
00150        PRINT:"T,P,ZP,PHI,ZPP,CP";READ:T,P,ZP,PHI,ZPP,CP
00155   10   PRINT:"SHOULD 1ST. SLN DOMINATE?";READ:FIRST
00160        PRINT:"IS DATA SOURCE ON FILE?";READ:FILE
00170        IF(FILE.EQ."NO") GO TO 11
00180        READ("FILE1",1) NT
00190     1  FORMAT(I5)
00200        READ("FILE1",2) (R(I),V(I),I=1,NT)
00210     2  FORMAT(E16.8,E11.3)
00220        GO TO 12
00230    11  PRINT:"NO. DATA PTS.";READ:NT
00240        PRINT:"RANGE AND VOLTAGE"
00250        PRINT:" "
00260        READ:(R(I),V(I),I=1,NT)
00261        PRINT:" "
00270    12  CONTINUE
```

```
00290       K=CAPR/2.*SE0*C*A*E
00300       PHI=PHI/57.2958
00310       SINP=SIN(PHI)
00311       TEST=ABS(SINP)
00312       IF(TEST.LT.1.E-10) SINP=1.E-10
00320       T1=CP*SGMT
00330       T2=2.*(SGR*N0)*T0/T*P/P0
00340       T3=SINP**2/3.
00350       T5=-2.3026*SINP
00360       T4=-ZP/T5
00370       T6=(SGRT*N0)*T0/T*P/P0
00380       Y4=-2.*CP*SGM
00390       S=0.0
00400       PRINT 3
00410     3 FORMAT(//6X,"R",11X,"V",11X,"M"//)
00420       DO 100 I=1,NT
00430       Y1=(V(I)/T1)*(R(I)**2/K)
00440       EX=T5*(R(I)/ZP)
00450       TEST=ABS(EX)
00460       IF(TEST.GT..01) GO TO 40
00470       SUM=0.0
00480       TRM=EX
00490       FI=1.
00500    30 SUM=SUM+TRM
00510       TEST=ABS(TRM/SUM)
00520       IF(TEST.LE.1.E-06) GO TO 50
00530       FI=FI+1.
00540       IF(FI.GT.20.) CALL ERROR(4,MSG1)
00550       TRM=TRM/FI*EX
00560       GO TO 30
00570    40 SUM=EXP(EX)-1.
00580    50 Y2=T2*((-ZPP*R(I)**3)*T3-T4*SUM)
00590       Y3=T6/T1*(3.*T3*(-ZPP*R(I)**2)+EXP(T5*(R(I)/ZP)))
00600       IF(I.EQ.1) DELR=R(1)
00610       IF(I.GT.1) DELR=(R(I)-R(I-1))/2.
00620       IF(I.EQ.1) C1=Y1*EXP(Y2)
00630       IF(I.GT.1) S=S+M*DELR
00640       IF(I.GT.1) C1=Y1*EXP(Y2-Y4*S)
00650       C2=Y3
00660       C3=Y4*DELR
00670       MP=-(1./C3+C2)
00680       MPP=MP-1./C3
00685       J=1
00690       IF(MP.GT.0.) GO TO 60
00700       IF(C1.GT.C2) CALL ERROR(4,MSG2)
00710       M=0.
00720       IF(MPP.GT.0.) M=MPP
00740       GO TO 70
00750    60 FMP=(MP+C2)*EXP(C3*MP)
00760       IF(C1.GT.FMP) CALL ERROR(4,MSG3)
```

```
00770        IF(FIRST.EQ."N") GO TO 65
00780        M=0.
00790        IF(C1.LE.C2) GO TO 80
00800        GO TO 70
00810     65 M=MPP
00820     70 FM=(M+C2)*EXP(C3*M)
00830        FPM=(1.+C3*(M+C2))*EXP(C3*M)
00840        SAVM=M
00850        M=SAVM+(C1-FM)/FPM
00860        TEST=ABS((M-SAVM)/(M+SAVM))
00870        J=J+1
00880        IF(J.GT.50) CALL ERROR(4,MSG4)
00890         IF(TEST.GT.1.E-06) GO TO 70
00900     80 S=S+M*DELR
00910    100 PRINT 4,R(I),V(I),M
00920      4 FORMAT(1P3E12.4)
00930        GO TO 10
00960        END
```

In order to test the RANGM program listed above, it was found to be convenient to write an additional program called RANGV which will compute m_i given V_i and r_i. This program simply solves equation (17) for V_i using the procedures outlined in the previous discussion of RANGM for the evaluation of the integrals. This computation requires no iteration or choice of solutions since V_i is uniquely specified by m_i and r_i. The input is the same as for RANGM with the exception that the data input are now r_i and m_i. The program prints out r_i, V_i, and m_i the same as RANGM. A complete listing of the program is shown below.


```
READY
%LIST RANGV                    RANGV

01/13/70   17.302

00010        DIMENSION M(200),R(200),V(200)
00020         REAL N0,M,K
```

```
00030       ASCII MSG1,RTFL
00040       CALL SETERR(15)
00050        MSG1="ERR1"
00060       C=2.9971E+10
00070       SGR=1.6692E-27
00080       SGRT=1.9925E-28
00090       N0=2.6871E+19
 100        T0=491.7
00110       P0=29.921
00120       PRINT:"R,SE0,A,E,SGM,SGMT";READ:CAPR,SE0,A,E,SGM,SGMT
00130       PRINT:"T,P,ZP,PHI,ZPP,CP";READ:T,P,ZP,PHI,ZPP,CP
00140    10 PRINT:"WRITE A BCD FILE?";READ:RTFL
00210       PRINT:"NO. DATA PTS.";READ:NT
00220       PRINT:"RANGE AND MASS"
00221       PRINT:" "
00240       READ:(R(I),M(I),I=1,NT)
00250       K=CAPR/2.*SE0*C*A*E
00260       PHI=PHI/57.2958
00270       SINP=SIN(PHI)
00271       TEST=ABS(SINP)
00272       IF(TEST.LT.1.E-10) SINP=1.E-10
00280       T1=CP*SGMT
00290       T2=2.*(SGR*N0)*T0/T*P/P0
00300       T3=SINP**2/3.
00310       T5=-2.3026*SINP
00320       T4=-ZP/T5
00330       T6=(SGRT*N0)*T0/T*P/P0
00340       PRINT 2
00350     2 FORMAT(//6X,"R",11X,"V",11X,"M"//)
00360       DO 100 I=1,NT
00370       IF(I.EQ.1) S=M(1)*R(1)
00380       IF(I.NE.1) S=S+(M(I)+M(I-1))/2.*(R(I)-R(I-1))
00390       EX=T5*(R(I)/ZP)
00400       TEST=ABS(EX)
00410       IF(TEST.GT..01) GO TO 40
00420       SUM=0.0
00430       TRM=EX
00440       FI=1.
00450    30 SUM=SUM+TRM
00460       TEST=ABS(TRM/SUM)
00470       IF(TEST.LE.1.E-06) GO TO 50
00480       FI=FI+1.
00490       IF(FI.GT.20.) CALL ERROR(4,MSG1)
00495       TRM=TRM/FI*EX
00510       GO TO 30
00520    40 SUM=EXP(EX)-1.
00530    50 TRM=T2/2.*((-ZPP*R(I)**3)*T3-T4*SUM)
00540       TRM=(TRM+CP*SGM*S)
00550       TRM=EXP(-2.*TRM)
00560       FCT=K/R(I)**2*(T1*M(I)+T6*((-ZPP*R(I)**2)*3.*T3
00570        +EXP(T5*(R(I)/ZP))))
```

RECOMM

```
00580        V(I)=FCT*TRM
00590   100  PRINT 3,R(I),V(I),M(I)
00600     3  FORMAT(1P3E12.4)
00605        IF(RTFL.EQ."NO") GO TO 10
00606        WRITE("FILE1",4) NT
00607     4  FORMAT(I5)
00610        WRITE("FILE1",5) (R(I),V(I),I=1,NT)
00611     5  FORMAT(E16.8,E11.3)
00620        GO TO 10
00630        END
```

Reference

1. J. V. Uspensky, Theory of Equations, p. 175, McGraw-Hill, New York (1948).

APPENDIX D

MISCELLANEOUS SYSTEM PHOTOGRAPHS

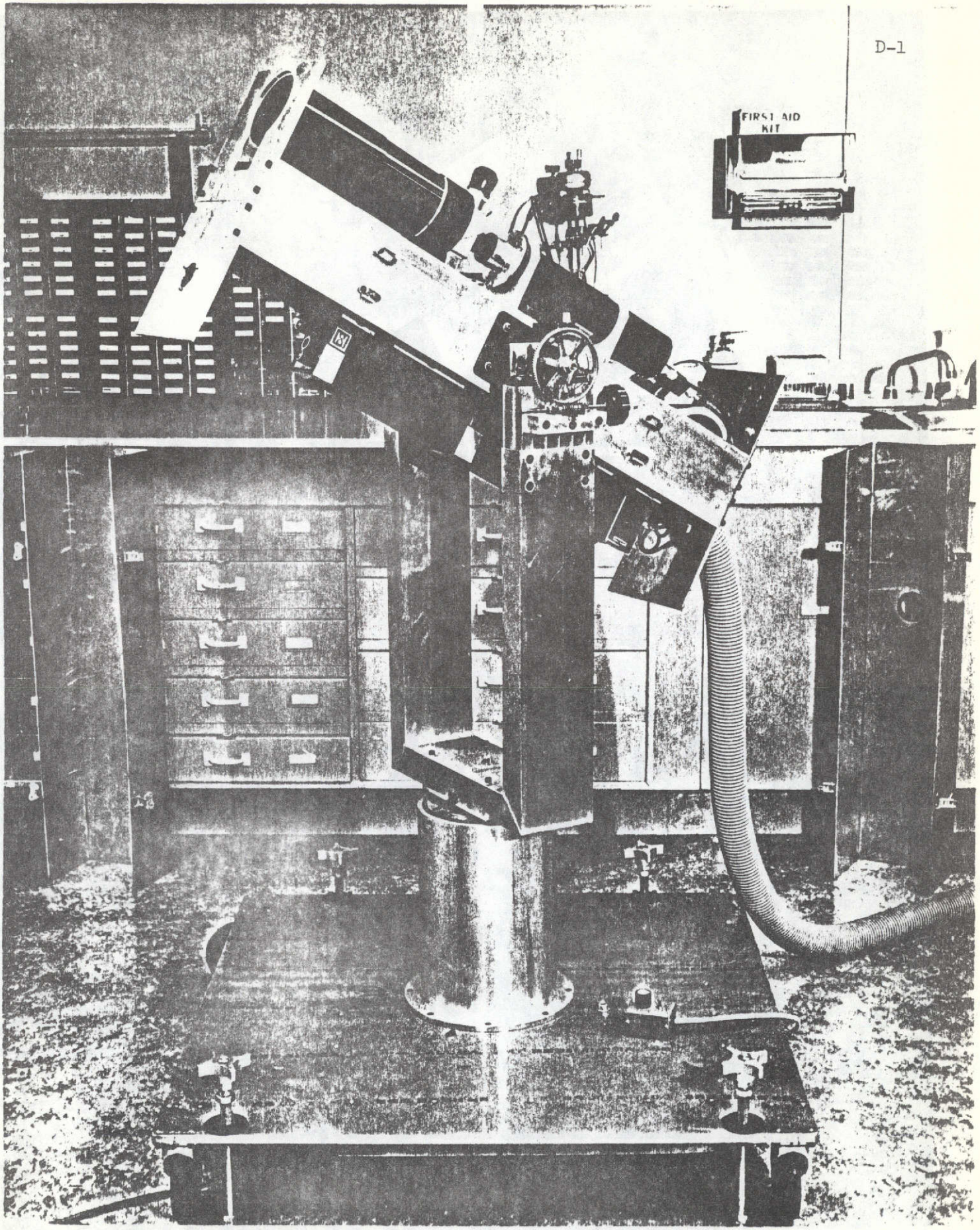

Figure D-1 Receiver and transmitter mounted on azimuth and elevation positioner with dust covers removed.

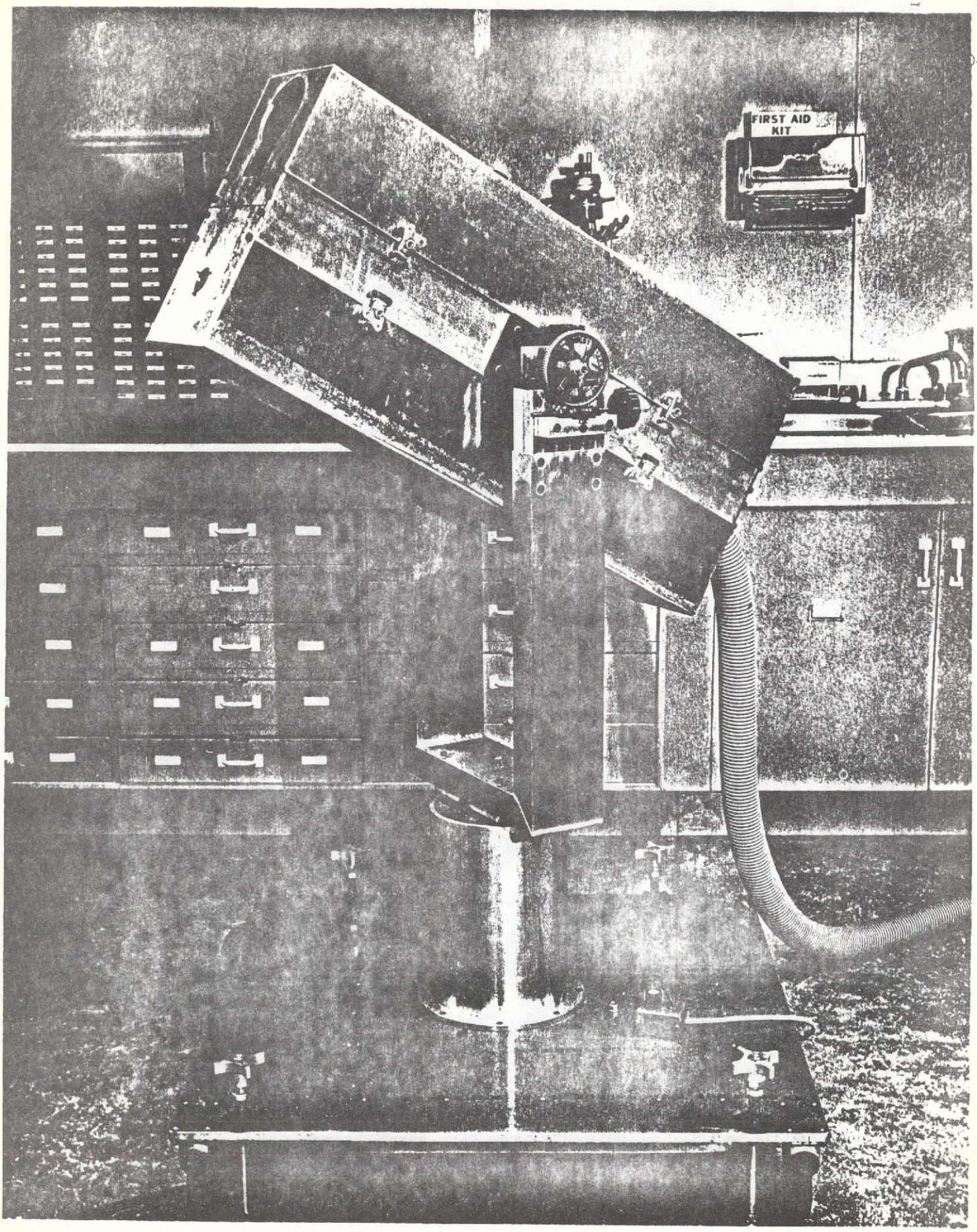

Figure D-2 Receiver and transmitter mounted on azimuth and elevation positioner with dust covers secured.

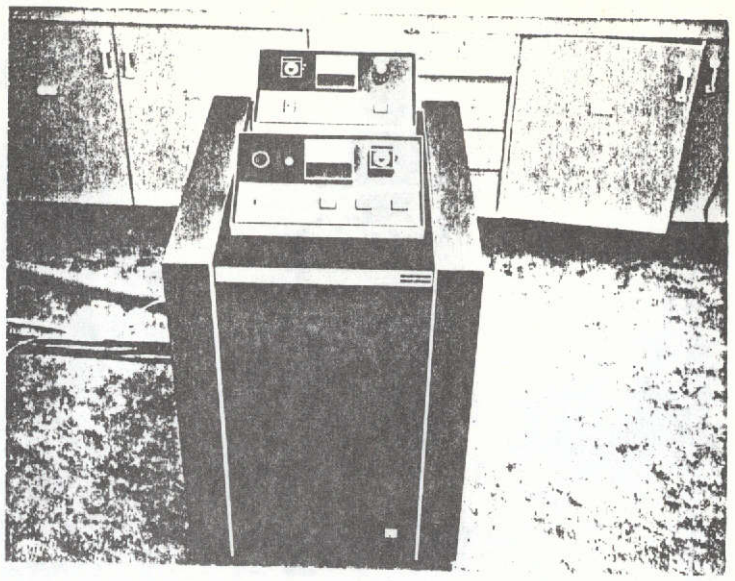

Figure D-3 Laser system power supply and remote stations for control of laser and Pockels cell.

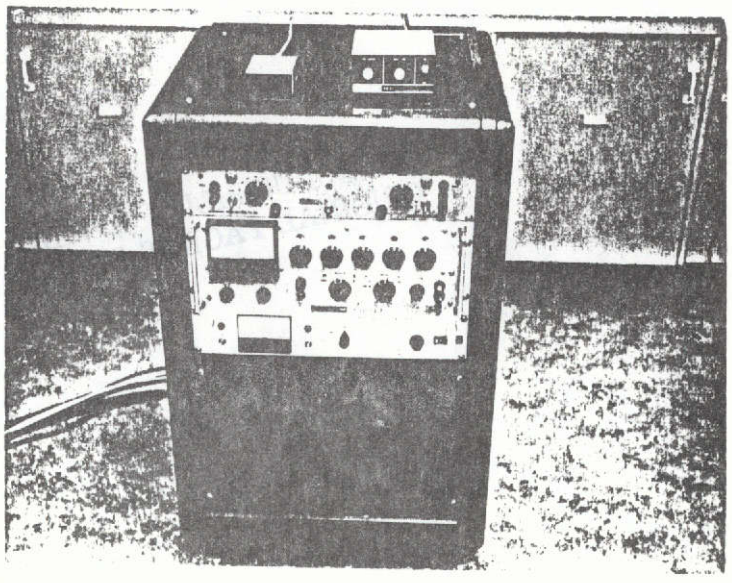

Figure D-4 Electronics console containing Photomultiplier tube power supplies and laser power meter (on top of console_.

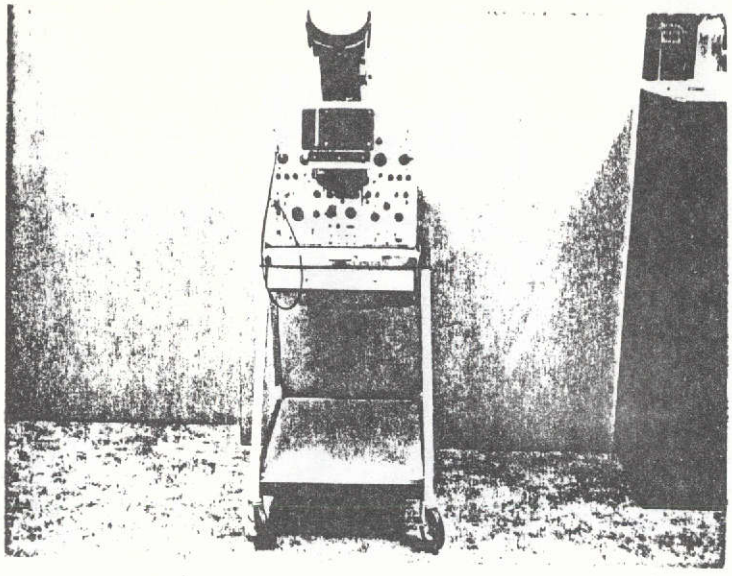

Figure D-5 Tektronix model 556 Dual Beam Oscilloscope and Tektronix C12 Camera.